Proceedings of ASME Turbo Expo 2011
GT2011
June 6-10, 2011, Vancouver, British Columbia, Canada

GT2011-46122

INVESTIGATION OF PRE-STALL BEHAVIOR IN AN AXIAL COMPRESSOR ROTOR-PART 2 : FLOW MECHANISM OF SPIKE EMERGENCE

Yanhui Wu, Qingpeng Li, Jiangtao Tian, Wuli Chu
School of Power and Energy, Northwestern Polytechnical University
Xi'an, Shanxi, P.R. China

ABSTRACT

In order to investigate the pre-stall behavior of an axial flow compressor rotor, which was experimentally observed with spike-type stall inception, systematical experimental and whole-passage simulations were laid out to analyze the internal flow fields in the test rotor. In this part, emphases were put on the analyses of the flowfields of whole-passage simulation, which finally diverged, and the objective was to uncover the flow mechanism of short length scale disturbance (or spike) emergence.

The numerical result demonstrated that the test rotor was of spike-type stall initiation. The numerical probes arranged ahead of the rotor to monitor the static pressure variation showed there first appear two pips on the curves. After one rotor revolution, there was only left one pip spreading at about 33.3% rotor speed. This propagation speed was almost same as that of spike observed in experiments. The further analysis of the flow field revealed a concentrated blockage sector on the flow annuls ahead of rotor developed gradually with the self-adjustment of flowfields. The two pins on monitoring curves corresponded to two local blockage regions in near-tip passages, and were designated as B1 and B2 respectively. The correlation between the TSVs in the preceding and native passages was the flow mechanism for propagation of B2 and B1, thereby leading to their spread speed approximate to the active period of TSV in one passage. Furthermore, the self-sustained unsteady cycle of TSV was the underlying flow mechanism for the occurrence of the so-called "tip clearance spillage flow" and "tip clearance backflow". Because B2 was the tip-front of the blockage sector, TSV associated with its propagation became stronger and stronger so that the "tip clearance backflow" induced by it was capable of spilling into the next passage below the blade tip. This phenomenon was regarded as the threshold event that B2 started to evolve into a spike. The distinctive flow feature during the development stage of spike was the occurrence of a separation focus on the suction side in the affected passages, which changed the self-sustained unsteady cycle of TSV substantially. A three-dimensional vortex originating from this focus led to a drastic increase in the strength of TSV, which in turn led to a rapid increase in the "tip clearance backflow" induced by TSV and the radial extent of spillage flow.

INTRODUCTION

It is well known that tip clearance flow and its associated vortex affect the performance and stability of axial flow compressors. Therefore, much effort was made to explore the flow mechanism of tip clearance flow and it possible link with stall inception process in axial compressors. Inoue et al. [1-2] measured tip leakage flow fields behind and inside a low-speed compressor rotor at design condition. They found the interaction between tip leakage flow and incoming flow forced tip leakage flow rolling up into a slender vortex, which can be clearly seen a coiling of secondary vectors near the casing. However, when they conducted measurement on the same test rig [3, 4] at near stall condition, the abnormal flow phenomena were observed: the coiling of secondary vectors near the casing disappeared, while the low-energy fluid were spread out to about 60% percent of span. This inexplicable behavior of tip leakage vortex remained an unresolved puzzle during that period. Benefiting from the development of CFD techniques, Furukawa et al. [5] proposed a reasonable interpretation of the above abnormal phenomena from a viewpoint of "vortex breakdown" through analyzing the simulated flow field in detail. Besides, Bialjie et al [6] showed the evidence of the breakdown of tip leakage vortex based on SPIV measurements in a low-speed large scale axial flow compressor test rig.

When compressors approach the stall limit, the unsteadiness of flow fields near casing became more and more dominant. Furukawa et al. [7] and Yamada et al [8] numerically investigated unsteady behaviors in a low-seed and a transonic axial compressor rotor. They found the breakdown of tip leakage vortex was responsible for the unsteadiness of flow fields near the casing. However, experimental and numerical

investigations conducted by März et al. [9] revealed that a vortex structure formed near the leading edge plane, which was the result of interactions among the classical tip-clearance flow, axially reverse end-wall flow, and incoming flow. The formation and movement of this vortex seemed to be the main causes of unsteadiness when the test low-speed compressor operated at near stall conditions.

Besides, efforts on understanding the onset of rotating stall/surge have been another research subject with the rapid advance of computer and CFD technology. Recent unsteady simulations to stall have achieved many valuable findings of flow structure leading to stall. Hoying et al. [10] first successfully simulated the short length-scale (or spike) rotating stall inception for the low-speed version of E^3 compressor. They found that the stall inception is a result of the motion of tip clearance vortex moving upstream of the blade passage when the vortex trajectory was aligned with the blade leading edge plane. Though systematical singe-passage and multi-passage simulations, Vo et al. [11] further proposed two conditions necessary for the formation of spike disturbance: one is that the spillage of tip clearance flow to the adjacent blade passage ahead of the rotor leading edge and below the blade tip; the other is the initiation of backflow stemming from the leakage fluid in adjacent passages at the trailing edge plane. Hereafter, the two necessary conditions will be referred as "tip clearance spillage flow" and "tip clearance backflow". It should be noted that the sequence of these two threshold event may alter, but both must be present for compressors exhibiting spike disturbances. Hah et al. [12] conducted full-annulus computations to investigate the short length-scale stall inception in a transonic axial compressor rotor, and their observations were consistent with the two condition proposed by Vo et al. [11]. Furthermore, Chen et al. [13] carried out the full-annulus calculations using high-performance parallel computing to study the pre-stall behavior of a transonic axial compressor stage. Their simulations demonstrated the development of the rotating stall from the growth of rotating instabilities, i.e., a rotating long-length disturbance followed by a spike-type breakdown. Further flow field analysis indicated that the spike instabilities occurred when the trajectory of tip clearance flow is vertical to the axial direction.

The above investigations just focus on the description of flow phenomena associated with spiked initiated rotating stall: the so-called "tip clearance spillage flow" and "tip clearance backflow". No attempts were made to explore the exact flow mechanism underlying these phenomena. It is no doubt that the instantaneous complicated flow structures near casing at near stall condition are closely related to the onset of rotating stall for tip critical compressors. Expressed in another way, what is the flow mechanism of unsteadiness of tip clearance flow at near stall conditions, and how it links with the spike disturbances emerging from the flow fields? This is the motivation for the current study.

The current study is based on a high-speed small-scale axial compressor rotor, which had been experimentally observed to exhibit the spike type stall inception. In order to get the answer of the above questions, the work reported here divide into two parts. Part I presented the experimental and whole-passage numerical investigations, and the aim was to uncover the flow mechanism of unsteadiness of tip clearance flow at near stall conditions. Based on the results from Part I, whole-passage unsteady simulation beyond the last stable point was further analyzed in Part II, and the objective was to explore the linkage between the unsteady nature of tip clearance flow and the spike emergence, i.e., the flow mechanism of spike emergence.

TEST COMPRESSOR ROTOR

The present work was performed on the isolated axial compressor rotor test rig in Northwestern Polytechnical University at Xi'an. Figure 1 showed a cross-sectional diagram of this stand. It consisted of a DC motor (250 KW), an accelerator or gearbox, a torque meter, a test section, an orifice plate flow meter, a discharge duct, and a throttle cone. The test rotor was isolated from the stator to avoid interaction effects generated by the presence of a downstream stator blade row.

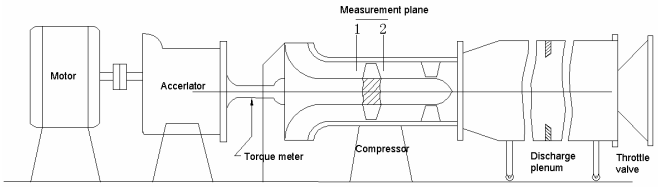

Figure 1 Cross-sectional diagram of the test rig.

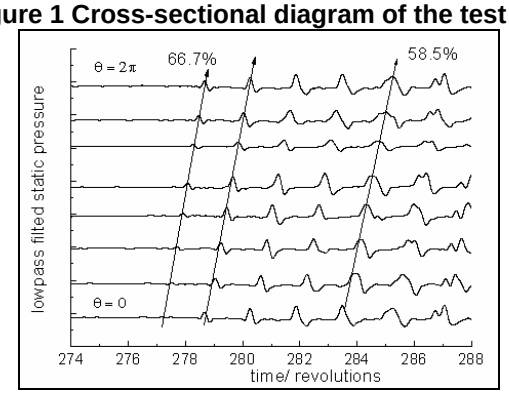

Figure 2 Typical stalling pattern of the test rotor

The hub/tip ratio of the rotor is 0.6, with the blade tip diameter of 298 mm. The rotor blade has Russia K70 series profile sections. The blade tip section of the rotor has the solidity of 0.961 and chord length of 30 mm. The nominal tip clearance is 0.3 mm (1.0 percent tip chord or 0.52 percent blade height), and it can be varied by exchanging casing segments with the rotor diameter remaining constant. Details of design specifications can refer to Xingen et al. [14]. Due to its tip critical nature, this rig has been widely used to test various kinds of casing treatment to determine their effectiveness on stall margin improvement (for example, Xingeng Lu et al. [14] Yanhui Wu et al. [15]). Recently, Lu [16] arranged 8 high-response pressure transducers ahead of rotor tip leading edge to

detect pressure fluctuations during instability onset with steady-state clean inlet. The measurements were conducted at corrected rotor speed of 8130 rpm with two different clearance gaps of 1.0%, and 1.7% tip chord (or 0.52%, and 0.86% blade height). At all tested cases, the stalling pattern of the test rotor was similar, and the compressor showed a spike-type stall inception. Figure 2 illustrated the stalling pattern of the test rotor with the tip gap of 0.86% blade height. The propagation velocity of spike was about 66.7% rotor speed at beginning. and then quickly transitioned into rotating stall cell within about 3 rotor revolutions, and the final speed of rotating stall cell was about 58.5%.

However, the fundamental flow mechanisms that lead to stall inception are not well understood by measurements due to the small-scale of this rig. A series of computational investigations, including steady and unsteady numerical simulations, has been therefore laid out to achieve this goal. Yanhui wu et al. [17] conducted steady single-passage simulations for this test rotor. After validating simulation results with available experimental data, the numerically obtained flowfields were analyzed to identify the behavior of tip leakage flow. It was found that the breakdown of the leakage vortex occurred inside the rotor passage at near stall conditions. Due to the vortex breakdown, a low-velocity region developed along the vortex core, thus producing a large blockage effect on incoming flow near the pressure side of the passage. Sparked by the numerical investigations conducted by Vo [11], the similar single-passage unsteady computations were further carried out by Yanhui wu [18] to assess the unsteady behavior of tip clearance flow, and to identify the threshold flow event leading to the spike initiated rotating stall. It was found that the "tip clearance spillage flow" did occur, but there was no "tip clearance backflow" during the stall inception process. The most predominant feature of flow fields near casing was that there was another distinctive vortex appeared at near stall conditions, apart from the breakdown of leakage vortex. This vortex, denoted as tip secondary vortex (TSV) probably arose from the interaction of the tip clearance flow among the adjacent blade passages. Due to the formation and movement of this vortex, the substantial unsteadiness of tip clearance flow occurred. In these simulations, the corrected rotor speed and the tip clearance size were set to be 8130 rpm and 1.7% tip chord, which were identical to those in Figure 2.

The experimental and numerical investigations in part I indicated that TSV did exist in tipflowfields at near stall conditions. Although asymmetry was introduced by truncation error, the activities of TSV in every passage were almost in-phases. The interface between incoming and tip clearance flow had the lower and upper limit due to the self-sustained activity of TSV during one unsteady cycle. At the last stable point from unsteady simulations, the upper limit of this interface reached the leading edge plane, which was one of criteria proposed by Vo [11] for spike initiated rotating stall. It could be inferred the upper limit of the interface between incoming and tip clearance flow would exceed the leading edge plane with the mass flow rate slightly decreased. Once this threshold event was initiated, the whole-annulus flow would fall into un-reversible unstable state, and the spike would emerge from the progressively developed non-axisymmetric flowfields.

Therefore, this paper focused on analyzing the solutions from unsteady simulation at flow condition with corrected mass flow rate of 2.70 kg/s, which finally diverged. The objective was to uncover the flow mechanism leading to the formation and development of spike disturbance.

NUMERICAL METHODOLOGY

Numerical schemes

Numerical simulations were performed by flow solver EURANUS. It computed the conservative Reynolds-averaged Navior-Stokes equations without *ad hoc* modeling of any flow phenomena other than models required for turbulence. The parallel version of this solver was implemented in a scalable form for using MPI message passing. The parallel implementation employed domain decomposition and supports general muti-block grids with arbitrary grid-block connectivity.

The equations were discretized in space using a cell-centered finite volume formulation. With a view to capture the tip leakage vortex sharply near the end-wall, a 2nd-order upwind scheme based on a flux difference splitting formulation (Roe, [19]) with the Van Albada limiter being implemented was chosen to evaluate the inviscid fluxes. The viscous fluxes were determined in a central differencing manner with Gauss's theorem. For steady simulations, the equations was sloved using an explicit four-stage Runge-Kutta method with local time step to obtain steady-state solutions. For unsteady simulations, equations were solved using the implicit dual time-stepping method proposed by Jameson [20], which consists in adding to the time-dependent equations pseudo-time derivative terms. This methodology retains the main advantages of the explicit time integration scheme already implemented for resolving steady-state problems. One equation turbulence model of Spalart-Allmaras [21] was employed to estimate the eddy viscosity. Local time stepping, implicit residual smoothing and multi-grid techniques were used to reduce the computation cost.

Physical time step for unsteady simulations was determined by rotational speed, and it took a rotor blade 20 time steps to passing through one pitch. Within each physical time step, 50 pseudo time iterations with a CFL number of 2-3 were performed.

Gridding

In the proper sense, the present study was the extension of numerical investigations conducted by Yanhui Wu [18], and the same single-passage grid should be adopted. However, limited by computation resources, another relatively coarse single-passage grid with true tip gap was built. To reduce the grid skewness, O4H topology was chosen to model the main flow region, and butterfly topology was used to model the true tip

gap. This grid consisted of 57 points along the annulus height, including 17 point along the radial height of the tip gap, thus having locally fine grid spacing near casing. The minimum grid spacing on the solid wall was 5×10^{-6} to evaluate the viscous fluxes at the wall by applying the no-slip and adiabatic conditions. This minimum grid spacing gave $y^{+}\leq3$ at the walls. The full-annulus grid was shown in Figure 3, which was generated by rotating and replicating the single-passage grid around the annulus. There were 30 blade passages for the entire grid with a total of 6,140,610 grid points, and the grid was partitioned into 210 blocks.

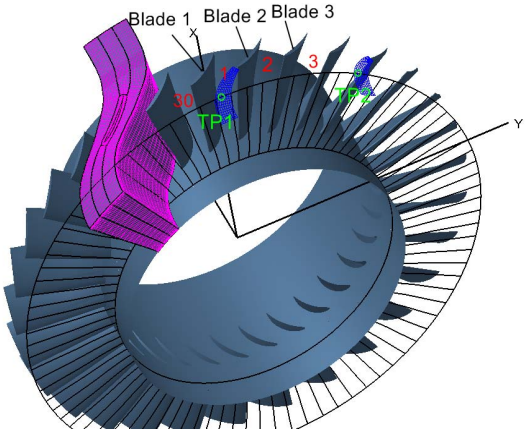

Figure 3 Blade passage and grid topology

For the convenience of the forthcoming analysis, the blades and passages were numbered as follows: the blade with x ordinate passing through its gravity center was named as Blade 1, then Blade 2 and so on, along the opposite rotational direction of the rotor; the passage between Blade 1 and 2 was named as Passage 1, then followed by Passage 2 between Blade 2 and 3 etc.

Boundary condition

No-slip and no-heat transfer conditions were imposed at solid boundaries. The flow was assumed to be steady-state at the inlet/outlet of the rotor. The flow angle, total pressure and total temperature were specified to be uniform across the whole inlet domain according to the experimental data. For steady calculations, the static pressure was set at the midspan, and the radial equilibrium equation was used to obtain the radial profile. Due to the substantial unsteadiness occurred at near stall conditions, the presetting pressure level at outlet boundary could not match the pressure variation arising from the unsteady flow. Therefore, the mass flow rate and initial static pressure were specified at outlet boundary for unsteady calculations, the successive pressure modification was calculated according to:

$$p^{new} = p^{old} + RELAXP\frac{\sqrt{\gamma_{gas}T_{ref}}}{L_{ref}^{2}}\left(Q^{actual} - Q^{imposed}\right)$$

Where L_{ref} and T_{ref} were the characteristic length and reference temperature, γ_{gas} and $RELAXP$ were the gas constant and relaxation factor, Q^{actual} and $Q^{imposed}$ were the mass flow rates calculated at the preceding time step, and specified at outlet boundary, P^{new} and p^{old} were the static pressures specified at the outlet boundary at the current and preceding time steps.

RESULTS AND DISCUSSION

Rotor characteristics

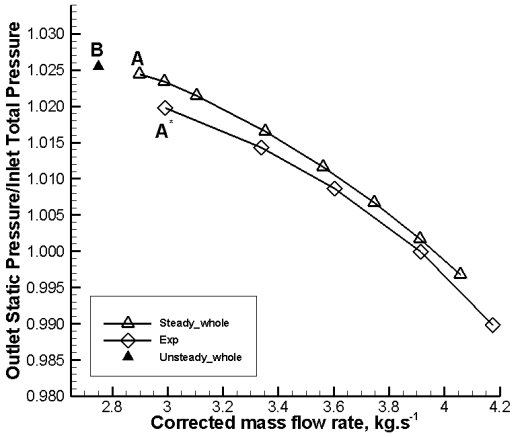

Figure 4 The comparison between the computed and experimental pressure rise characteristics

According to the model proposed by Camp et al. [22], the slope of total-to-static pressure rise characteristic was the key factor that determined the types of stall precursors for low-speed axial-flow compressors. The comparison between the computed and experimental total-to-static pressure rise characteristics was shown in Figure 4, where Point A* was the stall point from experiment, and Points A and B were the last stable points from steady and unsteady simulations. The pressure rise of Point B was the peak pressure in one unsteady cycle. The cause of slight over-prediction of stall point by unsteady simulations was discussed in Part I. Overall shape of the computed pressure rise characteristic was similar to that of experiment, and the slopes at last stable Points (B, and A*) remained negative. These negative slopes favored spike instability, which was consistent with experimental observation shown in Figure 2. Therefore, it was considered that the simulation could reasonably capture the flow mechanisms of spike emergence.

Monitoring results

Figure 5 showed the time histories of inlet/outlet mass flow rates at flow condition with corrected mass flow rate of 2.75 kg/s. The computed inlet mass flow rate reached the presetting value at outlet boundary after t=2.5 revolutions. This implied the outlet static pressure had been adjusted to a

reasonable value, and the computed flowfields approached a realistic state. The inlet/outlet mass flow sustained the level on the order of 2.70 kg/s between 2.5-4.45 revolution. Then, it slightly decreased followed by a sharp drop until the calculation diverged. The subsequent flowfield analyses indicated that the divergence of the solution was due to the presetting flow rate could not satisfy the situation that spike evolved into rotating stall cell because a drastic drop in flow rate would occur.

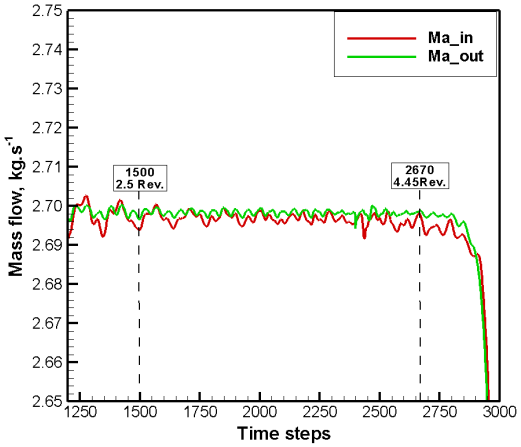

Figure 5 Time histories of inlet/outlet mass flow rate

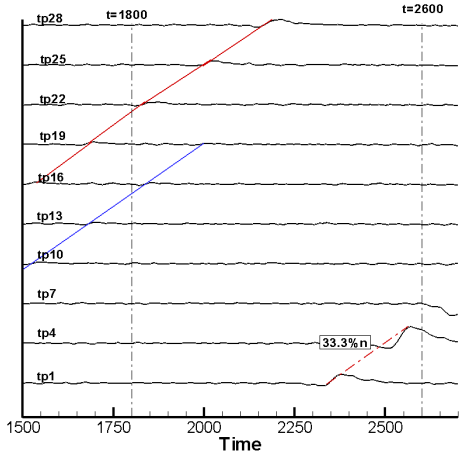

Figure 6 Static pressure traces at the location of the ten numerical probes

As described above, a probable time period of spike emergence was between 2.5 and 4.45 rotor revolutions. The time variations of static pressure during this period were detected by ten numerical probes, and the monitoring results were shown in Figure 6, where the pressure level was offset by the probe circumferential location. The ten numerical probes shown in Figure 3 were arranged every two blades at the axial location identical to that in measurement at 99% span. Because the flow equations were solved in the relative frame, the comparable results to those shown in Figure 2 could not be obtained. However, Figure 6 was still able to provide some important information.

There were two pins emerging from tip flowfields before t=2000, which corresponded to two local blockage regions. Hereafter, they were designated as B1 and B2 respectively, and their respective traces were marked by blue and red lines. The propagation speeds of B1 and B2 varied between 40%-36.4 rotor speed before t=1800. With the disappearance of B1, B2 gradually slowed down to the speed of 33.3% at about t=2100. Then, it nearly remained this speed till about t=2600. If viewed from the absolute frame, the propagation speed of B2 between t=2100-2600 is almost same as that of spike shown in Figure 2, leading to a deduction that spike was transitioned from B2.

Due to fact that B2 eventually evolved into a spike, the flowfields between t=1500-2600 were divided into two stages, which were defined by the vertical line at t=1800. The flowfields between t=1500-1800 was deemed as the embryonic stage of spike, while those between t=1800-2600 was the development stage of spike. Therefore, the analyses on the embryonic stage focused on uncovering the flow mechanism of spike emergence, while those on the development stage concentrated on identifying the flow features accompanied by the development of the spike.

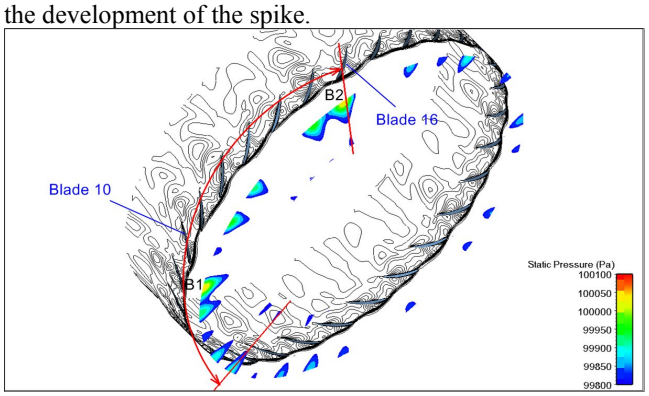

(a) t=1500

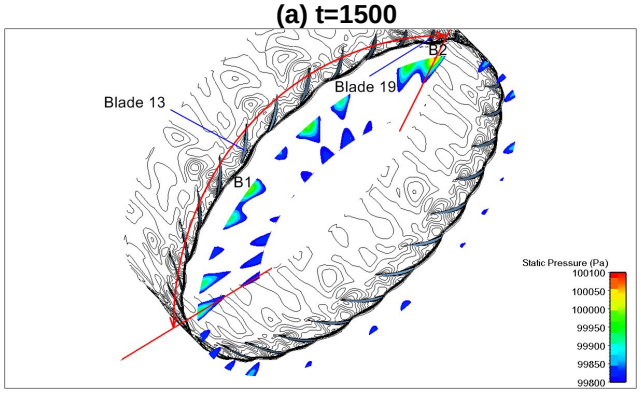

(b) t=1650

Figure 7 Static Distributions on the plane 100% tip axial chord ahead of rotor and entropy distributions on a surface of revolution at blade tip

Flow mechanism of spike emergence

The flowfields between t=1500-1650, in which B1 and B2 coexisted, were first examined. Due to the fact that B1 and B2 propagated at varying speed, the period of 50 time steps

was chosen to sketch the overall tendency of flowfield variation.

Figure 7 represented the static pressure distributions on the plane where the numerical probes located, and entropy distributions on a surface of revolution at blade tip. In contrast to flowfield at operating condition with mass flow of 2.75 kg/s, asymmetry across passages became dominant. The passages, which had relatively high pressure spot near tip, appeared the so-called "tip clearance spillage flow". It was noticeable that near-tip loading for a specific blade changed dynamically at different instants. At t=1500, an embryonic blockage sector, where the blockage effect near tip was much larger than that near hub, occurred between blades 6 and 16. This blockage sector occupied 1/3 flow annulus, and it rotated over a pitch along the circumference at about 50 time steps. This spatial flow pattern gradually strengthened at t=1650.

In this spatial blockage sector, there were two spots with extremely high pressure. At t=1500, they nearly pointed to the tips of Blades 10 and 16 respectively. In comparison with the monitoring results shown in Figure 6, it was obviously that the spot ahead of Blade 10 corresponded to B1, whereas the other ahead of Blade 16 corresponded to B2. As time elapsed, the two spots also rotated over a tip pitch at about an interval of 50 time steps. At instant t=1650, they arrived at locations nearly pointing to Blade 19 and Blade 13. The occurrence and development of this concentrated blockage sector provided prerequisite for a spike emergence.

The flowfield in the near-tip passages from t=1550 to t=1600 were closely examined to explore the underlying flow mechanism by which B2 and B1 rotated. As described in Part 1, the vortical motion of TLV and TSV induced two distinctive negative axial velocity regions on blade-to-blade section at tip, which could be used to identify the existence of these two vortices in current full-annulus analysis. Thus, the full-annulus negative axial velocity distributions on the blade-tip section, as well as the static pressure distributions identical to that shown in Figure 7, were presented in the center of Figure 8. Using these center pictures as indicators, the near-tip flow fields of Passage 16 and 17 were locally zoomed. The leakage streamlines were placed on the upper left corner, and the casing static pressure distributions were placed on the lower right corner. In addition, the limiting streamlines on the blade 17 were shown in Figure 9.The global view in conjunction with the locally zoomed view animated the complex flow structures associated with the propagation of B2:

At t=1550, there was a clearly negative axial velocity region on tip section of Passage 16, which was nearly perpendicular to the negative region induced by the TLV. This was the evidence for the existence of TSV. Due to the blockage effect caused by TSV, the leakage flow fluid forming TLV had to turn around it, and then convected downstream or crossed over the tip gap. The vortical motion of TSV induced a relatively low static pressure region near the pressure side of Passage 16. An impingement line on pressure side of blade 17 indicated the "tip clearance spillage flow" occurred.

At t=1560, the negative axial velocity region induced by the TSV diminished, and the relatively low static pressure region near the pressure side of Passage 16 disappeared. This meant the strength of TLV in Passage 16 decreased gradually as time elapsed. Therefore, it had no longer strong enough so as to influence the casing static pressure distribution. The space originally occupied by TSV was filled in the high pressure fluid from the rear part of Passage 16. This forced part of the fluid from TLV in passage 16 to impinge and cross over the tip gap of blade 17. This cross-over fluid had relatively large deficit in kinetic energy, and made contribution for the formation of TSV. TSV started to induce a dense pressure gradient region across the passage 17 near the trailing edge of blade 17, and the "tip clearance spillage flow" still occurred at this instant.

At t=1570, the leakage fluid from the TLV still entered into Passage 17 through radial gap and made contribution to the formation of TSV. TSV in Passage 17 became strong enough so that its front end induced a low pressure spot on casing. The rear end of the impingement leakage fluid approached the trailing edge of Blade 17, and the dense pressure gradient region already reached the outlet of blade 17. The "tip clearance spillage flow" disappeared accompanied by the disappearance of the leading edge impingement line on Blade 17. However, it occurred below the tip of Blade 18 due to the blockage effect arising from the stronger TSV in Passage 17.

At t=1580, part of the impingement fluid from TLV was relieved. Under the action of dense pressure gradient region induce by TSV, the so-called "tip clearance backflow" occurred.

At t=1590, the leakage fluid forming TLV in passage 16 totally moved out of the passage. Although TSV became weak as compared to that at t=1580, it was still able to induce "tip clearance backflow". The "tip clearance spillage flow" below the tip of blade 18 still appeared.

At t=1600, the "tip clearance backflow" totally disappeared, and the flow pattern in Passage 17 was nearly same as that in Passage 16 at t=1550.

From above analysis, it could be seen the propagation of B2 included the rear part of active period of TSV in Passage 16 and the fore part of active period of TSV in Passage 17. Consequently, the consuming time for B2 rotating over a tip pitch approximated to the active period of TSV in one passage. The divergence line on the suction side of Blade 17 indicated the near-tip loading in the affected passage is much larger those at flow condition with the corrected mass flow rate of 2.75 kg/s. As discussed in Part I, the active period of TSV would be lengthen with the tip loading increased. This was reason why the propagation speed of B2 decreased.

As for B1, it propagated from the leading edge of Blade 11 to leading edge of Blade 12 during the same period. The dynamic variation of negative axial velocity region on blade-tip section of passage 10 and 11 indicated that the flow mechanism for propagation of B1 was similar to that of B2.

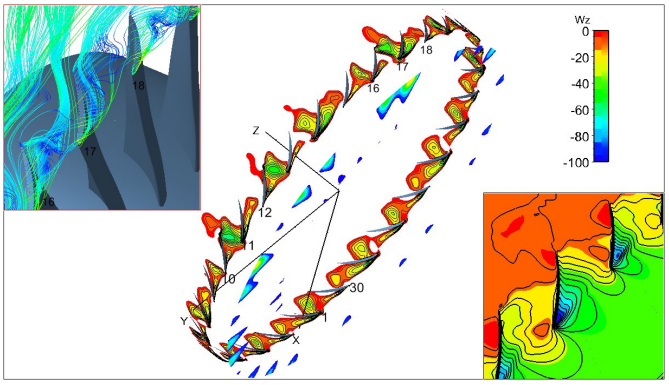

(a) t=1550

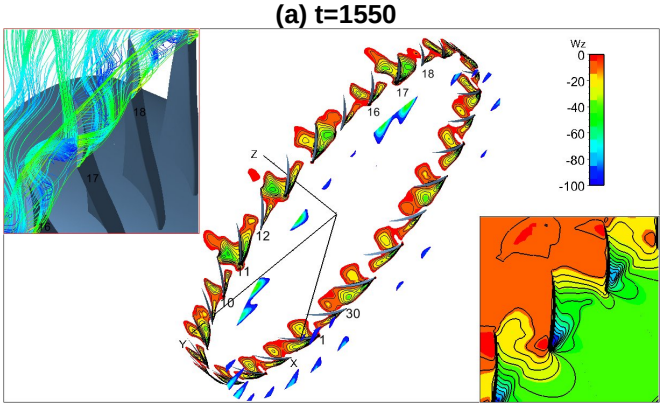

(b) t=1560

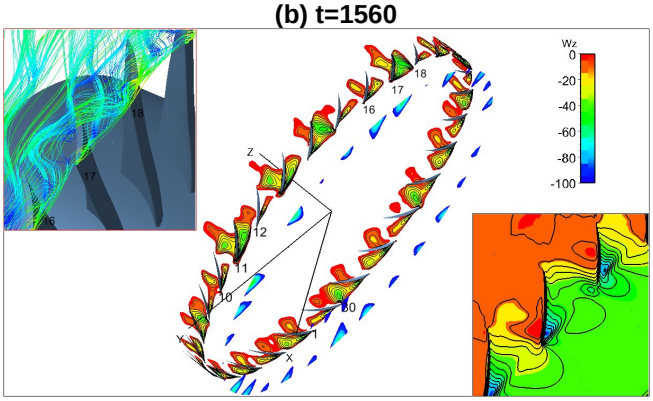

(c) t=1570

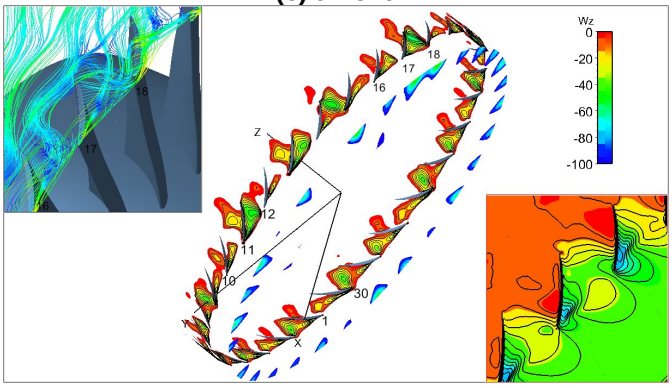

(d) t=1580

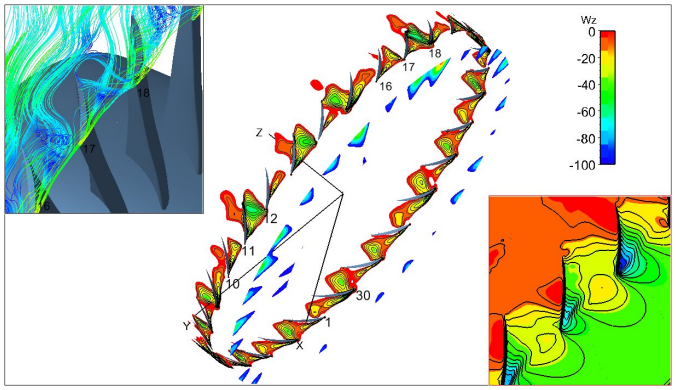

(e) t=1590

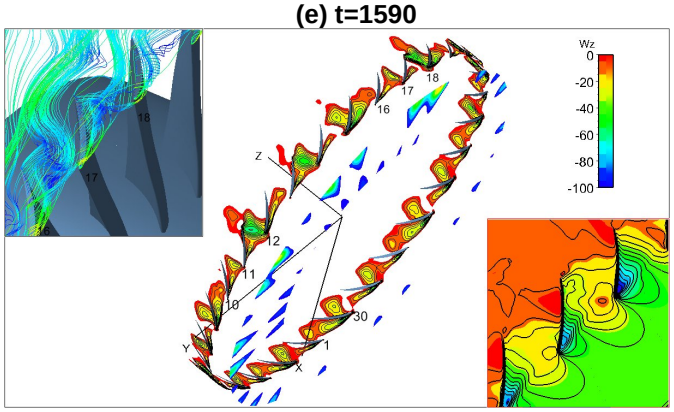

(f) t=1600

Figure 8 The detailed flow structure near tip from t=1550 to t=1600. Middle: distribution of negative axial velocity at blade tip section; upper left corner: locally zoomed leakage streamlines; lower right corner: locally zoomed casing static pressure distributions

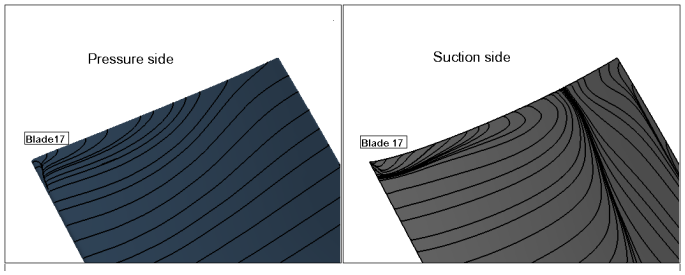

(a) t=1550

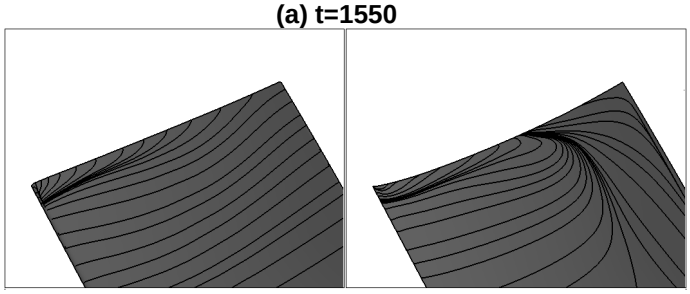

(b) t=1560

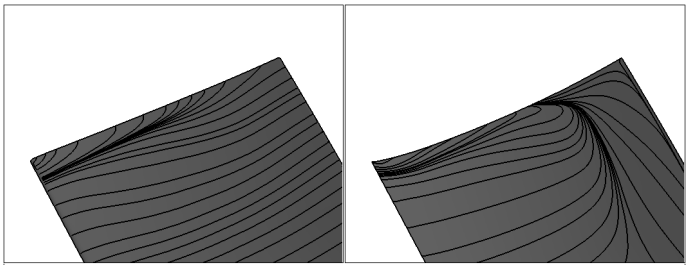

(c) t=1570

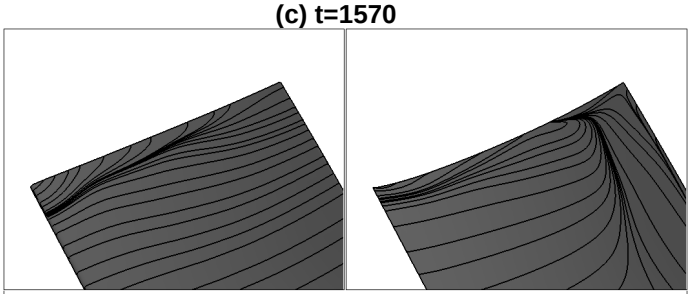

(d) t=1580

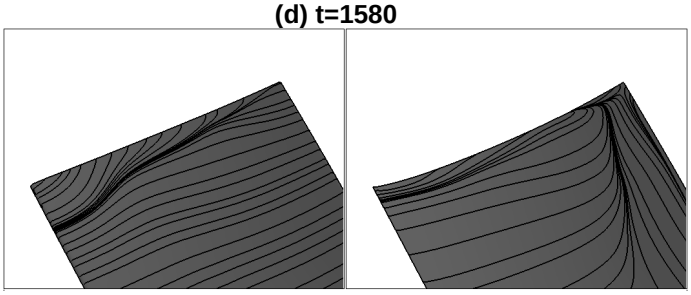

(e) t=1590

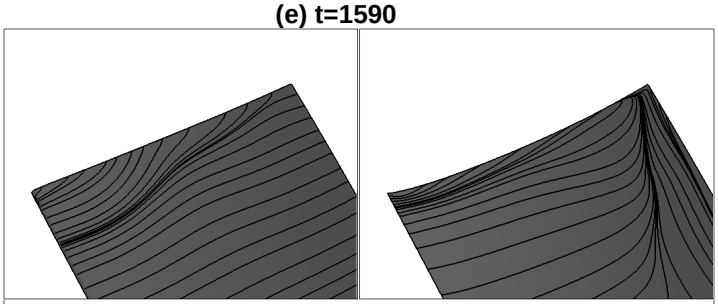

(f) t=1600

Figure 9 Limiting streamlines on the suction side and pressure side of Blade 17

In summary, the correlation between the TSVs in the preceding and native passages was the flow mechanism for propagation of B2 and B1. Furthermore, the blockage effect from TSV and the dense pressure gradient region induced by it were responsible for the occurrence of the so-called "tip clearance spillage flow" and "tip clearance backflow". That is, the self-sustained unsteady cycle of TSV was the underlying flow mechanism for the two criteria proposed by Vo. [11].

Because there were two severe tip blockage region coexisted in flowfield between t=1500-1800, the near-tip loading in each passage could not retain the same order. Thereby, the propagation speed of B2 and B1 varied from 40% to 36.4 rotor speed. However, with the self-adjustment of flowfield, the near-tip loading in the affected passages associated with propagation of B2 showed a tendency to increase.

Figure 10 showed the pressure distributions on the six axial-cuts and the locations of TSV at three instants just before the occurrence of "tip clearance backflow" associated with propagation of B2. The spiral motion of TSV induced a low pressure region on different axial cuts, especially on the first three axial cuts. As a result, the strength of TSV could be approximately evaluated from the areas of low pressure region on different axial cuts. It could be seen the TSV associated with the propagation of B2 also tended to become strong accordingly.

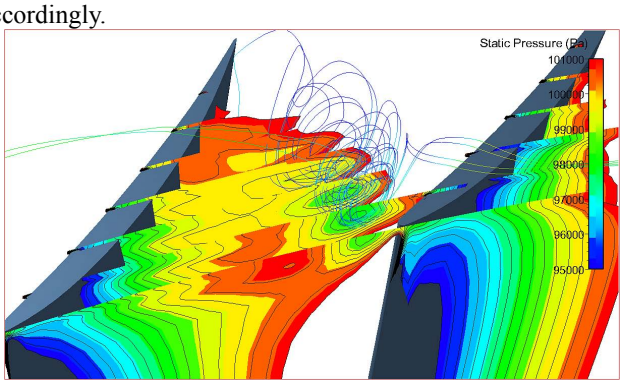

(a) t=1570

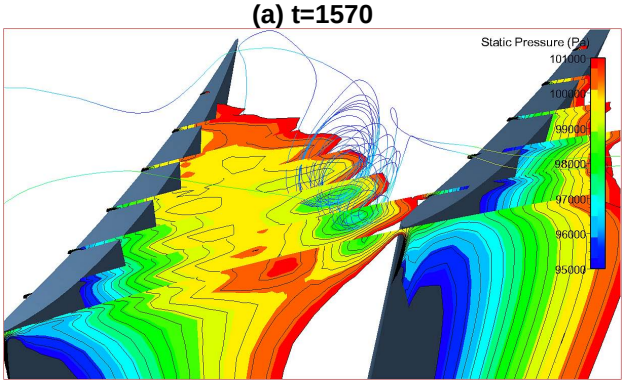

(b) t=1675

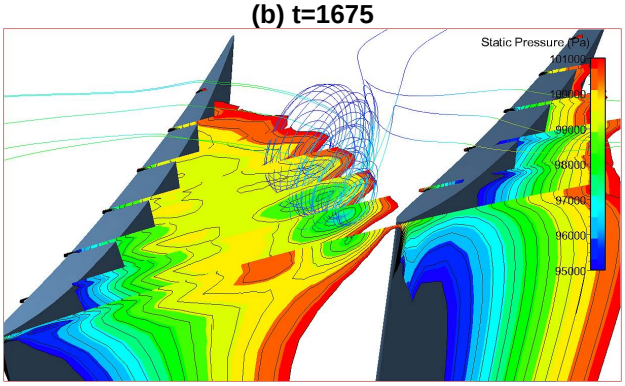

(c) t=1780

Figure 10 Pressure distributions on six axial-cuts at instants just before the occurrence of "tip clearance backflow" during t=1550-1800 associated with propagation of B2

During the time period between t=1500-1800, the "tip clearance backflow" originating from the preceding passage only convected downstream in the native passage whatever for B1 or B2. That is, the propagation of B1 and B2 concerned the behavior of tip clearance flow in two adjacent passages. However, with the strength of TSV associated with the propagation of B2 further increased, the "tip clearance backflow" induced by TSV began to leak into the next passage below the tip at leading edge, thus forming the "tip clearance back-spillage flow". Figure 11 illustrated this flow phenomenon at t=1910. Indeed, it appeared after t=1800, and was considered as the threshold event that B2 started to evolve into a spike because the propagation of B2 had now concerned the tip clearance flow behavior in three adjacent passages.

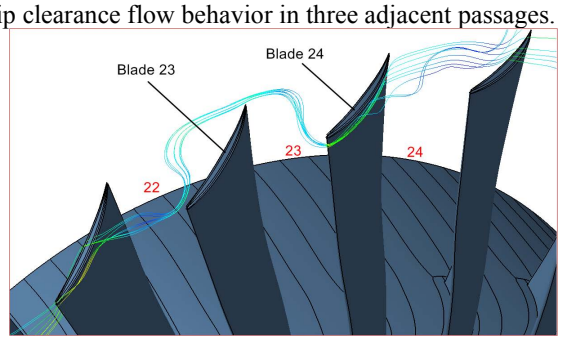

Figure 11 Illustration of "tip clearance backflow" forming "tip clearance spillage flow" at t=1910

Development of spike

The flow mechanism by which spike rotated during the period between t=1800-2600 was similar to its early stage except that the "tip clearance back-spillage flow" was involved.

Figure 12 presented the limiting streamlines on the suction sides of passages affected by TSV at t=1835, 2110, 2230, 2350, 2470 and 2590，which were the moments just before the occurrence of "tip clearance backflow ". With the disappearance of B1, the near-tip loading in the unaffected passages was gradually adjusted to the same order. Therefore, Figure 12 exhibited a gradual increase in the near-tip loading in affected passages associated with propagation of spike. This led to the propagation speed of spike gradually slowed down to 33.3% rotor speed at about t=2100, and then it continued to slow down till about t=2600.

Before t=2350, the flow mechanism for the formation of TSV and its self-sustained unsteady cycle were similar to those discussed in Part I. However, at t=2350 and after, the substantial change occurred. A separation focus with extremely low pressure around it appeared on the suction sides of affected passages. Figure 13 illustrated the vortical structures in the affected passages at t=2350 and 2590. At instant t=2350, the low-energy fluid from the suction boundary layer along the whole span accumulated the focus, and separated into the passage, thus forming a weak three-dimensional vortex. This vortex had the same rotation direction as that of TSV, and merged into the TSV. However, the strength of vortex from separation focus increased drastically at t=2590. This in turn led to the rapid increase in the strength of TSV.

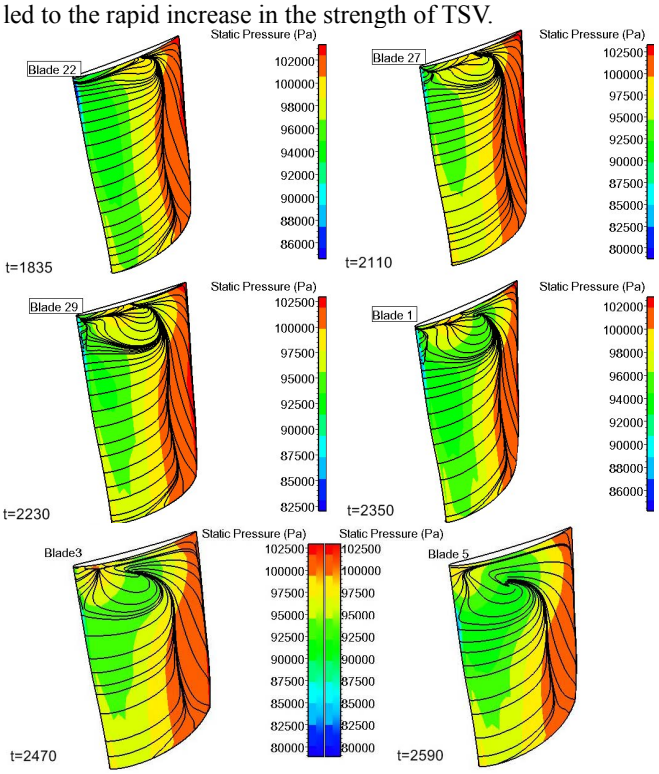

Figure 12 Limiting streamlines on the blade suction sides at t=1835,2110,2230, 2350，2470，2590

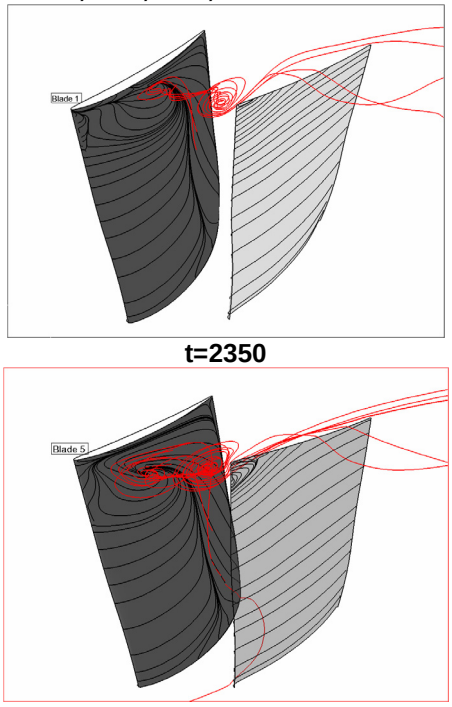

Figure 13 Vortical structures in the affected passage at instants t=2350 and 2590

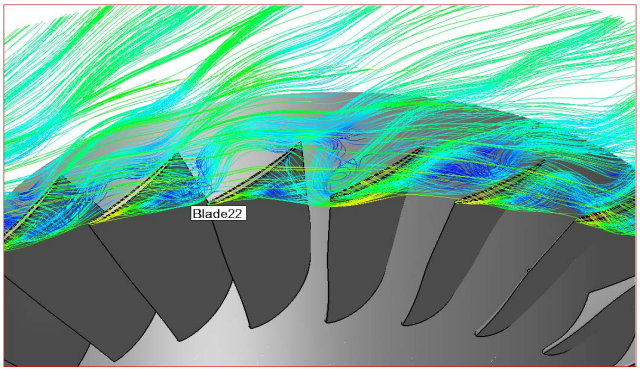

(a) t=1850

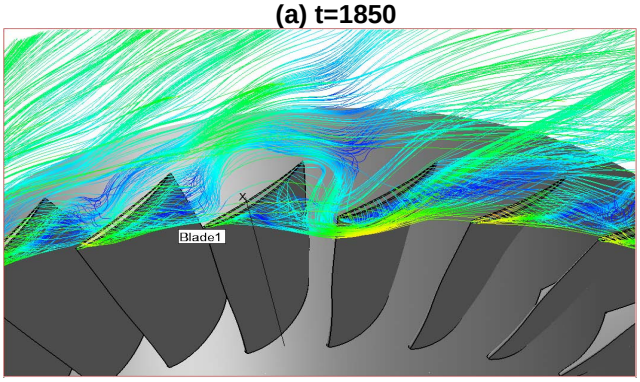

(b) t=2370

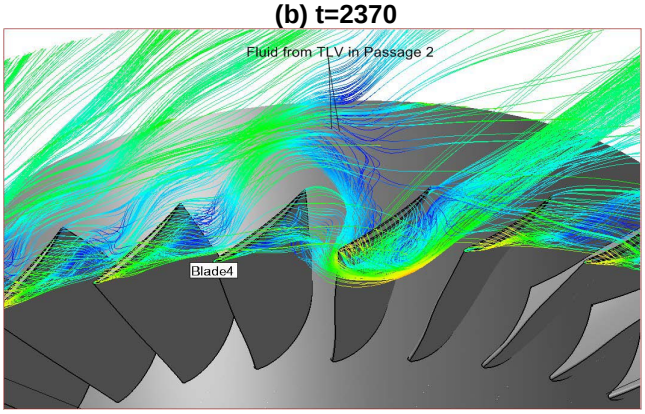

T=2570

Figure 14 the "tip clearance backflow" occurring at instants t=1850, 2370, 2570

Figure 14 showed the "tip clearance backflow" induced by TSV at t=1850, 2370, 2570. During the period between t=1800-2400 (one rotor revolution), the "tip clearance backflow" slowly built up. However, it increased drastically accompanied by the occurrence of separation focus in subsequent 1/3 rotor revolution. As shown in Figure 8(e), it was the combined blockage effect from the TSV and "tip clearance backflow" that made the pressure level of B2 reach its peak. Therefore, the magnitude of spike climbed slowly between t=1800-2400, while rised drastically between t=2400-2600 (Figure 6). These observations were consistent with that in measurement shown in Figure 2. At t=2570, not only all of the fluid from the TLV in Passage 3, but also a little fluid from TLV in Passage 2 formed the "tip clearance backflow". This indicated that the circumferential influencing region of spike had extended to four adjacent passages. The transition from spike into rotating stall cell was initiated from this point.

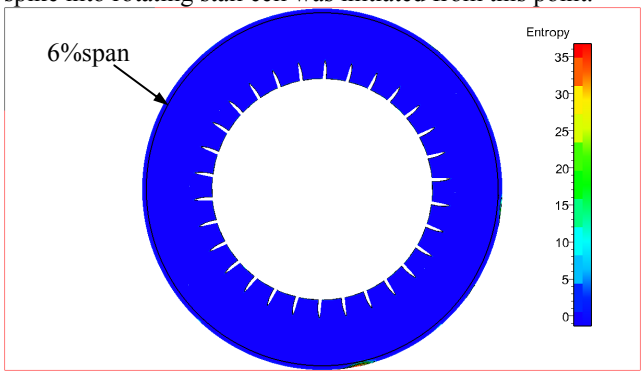

(a) t=1850

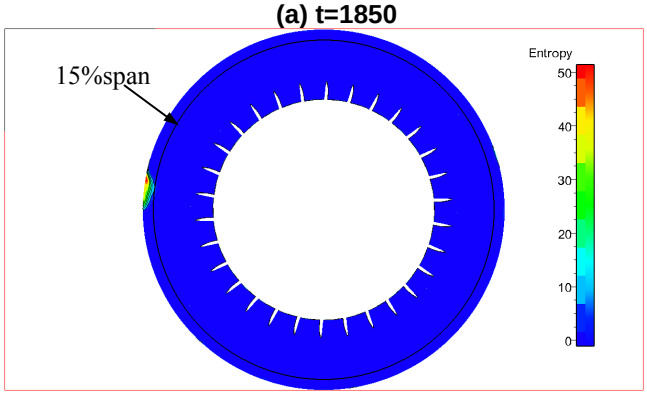

(b) t=2370

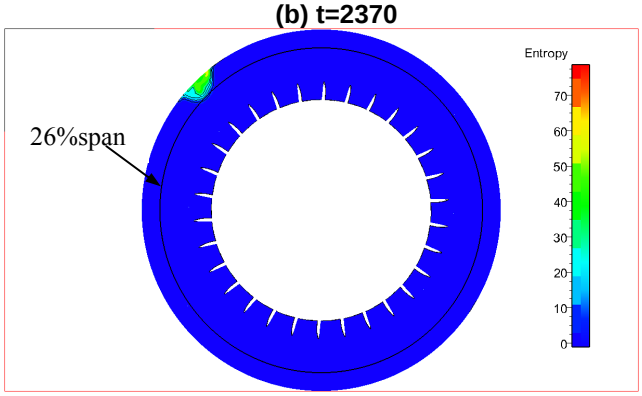

(c) t=2570

Figure 15 the "tip clearance backflow" occurring at t=1850, 2370, 2570

The high entropy region ahead of rotor reflected the radial extent of spillage flow. Figure 15 represented entropy distributions on the flow annulus ahead of rotor at 16% tip axial chord at the same instants as those in Figure 14. From t=1850 to t=2370, the radial extent of spillage flow increased from 6% to 15% span. However, it quickly extended to 26% span at t=2570. That is, the appearance of the separation focus on the suction side in affected passages led to the radial extent of spillage flow increased quickly, but it was still within 30% span before t=2600. This was consistent with the well accepted opinion that the radial extent of spike was less than 30% span.

CONCLUDING REMARKS

summary

In order to investigate the pre-stall behavior of an axial flow compressor rotor, which was experimentally observed with spike-type stall inception, systematical experimental and whole-passage simulations were laid out to analyze the internal flow fields in the test rotor. In this part, emphases were put on the analyses of the flowfields of whole-passage simulation, which finally diverged, and the following conclusions were drawn:

1) Overall shape of the computed total-to-static pressure rise characteristic matched well with that from experiment. The slope of the computed and experimental characteristics at the last stable point remained negative. The negative slope favored spike instability, which was proved by experimental observation.

2) The simulation also demonstrated the test rotor was of spike-type stall initiation. The numerical probes arranged ahead of the rotor to monitor the static pressure variation indicated there first appeared two pips on the curves, which spreading speed varied between 40%-36.4% rotor speeds. However, after one revolution, there was only left one pip, which spread at about 33.3% rotor speed during the succeeding one rotor revolution. This propagation speed was same as that of spike observed in experiment if viewed from the absolute frame.

3) The analysis of the flow field revealed that the interface between tip clearance flow and incoming flow was beyond the leading edge plane in most passages. With the self-adjustment of flowfields, a concentrated blockage sector on the flow annuls ahead of rotor developed gradually, where the blockage near tip was much larger than that near hub. The two pins on the monitoring curves were located in the middle and front of this blockage sector, and they corresponded to two local blockage regions in near-tip passages, which were designated as B1 and B2 respectively.

4) The correlation between the TSVs in the preceding and native passages was the flow mechanism for propagation of B2 and B1, thereby leading to their spread speed approximate to the active period of TSV in one passage. Furthermore, the self-sustained unsteady cycle of TSV was the underlying flow mechanism for the occurrence of the so-called "tip clearance spillage flow" and "tip clearance backflow".

5) Because B2 was the tip front of the blockage sector, TSV associated with its propagation became stronger and stronger so that the "tip clearance backflow" induced by it was capable of spilling into the next passage below the blade tip. This phenomenon was regarded as the threshold event that B2 started to evolve into a spike.

6) The distinctive flow feature during the development stage of spike is the occurrence of a separation focus on the suction side of the affected passage, which changed the self-sustained unsteady cycle of TSV substantially. Before its occurrence, the strength of TSV associated with propagation of spike increases gradually. This led to a slow accumulation of "tip clearance backflow" and a slow increase in the radial extent of "tip clearance spillage flow" in one rotor revolution. However, a three-dimensional vortex originating from this focus led to a drastic increase in the strength of TSV. Consequently, the "tip clearance backflow" and the radial extent of spillage flow increased drastically in the subsequent 1/3 rotor revolution.

What we learned

The simulation correlated well with the experimental observations from the two aspects. One was that the predicted speed of spike agreed well with that from experiment. The other was the circumferential and radial extent of spike was consistent with the well accepted opinions: 2-3 rotor pith and less than 30% span. Therefore, the current simulation reasonably captured the flow mechanisms of spike emergence. The current work in conjunction with investigations conducted by Jen-ping et al. [13] established the confidence of using CFD to investigate the pre-stall behavior of axial compressors.

ACKNOWLEDGMENTS

The authors would like to acknowledge the supports of National Natural Science Foundation of China, Grant No. 51076133, and the support of NPU Foundation for Fundamental Research, Grant No. W018101, and the support of Aeronautic Science Foundation, Granted No. 2010ZB53016.

REFERENCES

[1] Inoue, M., Kuroumaru, M., and Fukuhara, M., 1986, "Behavior of Tip Leakage Flow Behind an Axial Compressor Rotor," ASME Journal of Engineering for Gas Turbines and Power, Vol. 108, No. 1, pp. 7-14.

[2] Inoue, M., and Kuroumaru, M., 1989, "Structure of Tip Clearance Flow in an Isolated Axial Compressor Rotor," ASME Journal of Turbomachinery, Vol. 111, No. 3, pp. 250-256..

[3] Inoue, M., Kuroumaru, M., and Ando, Y., 1990, "Behavior of Tip Clearance Flow in Axial Flow Impellers at Low Flow Rate"Proceedings of the 3rd Japan-China Joint Conference on Fluid Machinery, Vol. II, pp. 179-186.

[4] Inoue, M., Kuroumaru, M., Iwamoto, T., and Ando, Y., 1991, "Detection of a Rotating Stall Precursor in Isolated Axial Flow Compressor Rotors," ASME Journal of Turbomachinery, Vol. 113, No. 2, pp. 281-289.

[5] Furukawa M, Inoue M, Saiki K, et al. The role of tip leakage vortex breakdown in compressor rotor aerodynamics. ASME Journal of Turbomachinery, 1999, 121(3): 469-480.

[6] Baojie, L., Xianjun, Y., Hongwei, W., Huoxing, L. etc, 2004, "Evolution of the Tip Leakage Vortex in an Axial Compressor Rotor", ASME-2004-53703.

[7] Furukawa M, Saiki K, Yamada K, et al. Unsteady flow behavior due to breakdown of tip leakage vortex in an axial compressor rotor at near-stall condition. ASME Paper, 2000-GT-666, 2000

[8] Yamada K, Furukawa M, Nakano K Unsteady three-dimensional flow phenomena due to breakdown of tip leakage vortex in a transonic axial compressor rotor. ASME Paper, 2004-GT-53745, 2004

[9] März, J., Hah, C., and Neise, W.An Experimental and Numerical Investigation into the Mechanisms of Rotating Instability, ASME Journal of Turbomachinery, 2002, 124:367~375

[10] Hoying D A, Tan C S, Vo H D, et al. Role of blade passage flow structures in axial compressor rotating stall inception[J]. ASME Journal of Turbomachinery, 1999, 121(4): 735-742

[11] Vo H H, Greitzer E M. Criteria for spike initiated rotating stall. ASME Paper, GT2005-68374, 2005.

[12] Hah C, Bergner J, Schiffer H., Short length-scale rotating stall inception in a transonic axial compressor-criteria and mechanism[R]. ASME Paper, GT2006-90045, 2006.

[13] Jen-ping C., Michael D. H., Pre-stall Behavior of a Transonic Axial Compressor Stage via Time-Accurate Numerical Simulation. ASME Paper, GT2007-27926.

[14] Xingen Lu, Wuli Chu, Junqiang Zhu. Numerical Investigations of the Coupled Flow through a Subsonic Compressor Rotor and Axial Skewed Slot. ASME Journal of Turbomachinery, 2007.

[15] Yanhui Wu, Wuli Chu, Haoguang Zhang. Parametric Investigation of Circumferential Grooves on Compressor Rotor Performance". ASME Journal of Fluid Engineering, 2010.

[16] Lu Xingeng, 2007, "Flow Instability and its Passive Control Strategies in Axial-flow Compressor," PH.D. Thesis, Northerwestern Polytechical University.

[17] Yanhui Wu, and Wuli, Chu., 2006, "Behavior of tip clearance flow in an axial flow compressor rotor", ASME Paper GT2006-90399.

[18] Yanhui Wu, Qingpeng Li, Wuli Chu. Numerical Investigation into Unsteady Behavior of Tip Clearance Flow and its possible link with stall inception. Proceedings of the Institution of Mechanical Engineers Part A-Journal of Power and Energy, 2009.

[19] Roe, P. L., 1981, "Approximate Riemann Solvers, Parameter Vectors and Difference Schemes", Journal of Computation Physics, Vol. 43, pp. 357-382.

[20] Jameson, A., 1991, "Time-dependent calculations using multigrid, with application to unsteady flows past airfoils and wings", AIAA-Paper 91-1596.

[21] Spalart, P. R., and Allmaras, S. R., 1992, "A one Equation Turbulence Model for Aerodynamic Flows," AIAA 92-0439.

[22] Camp, T.R. and Day, I.J., 1998, 'Study of Spike and Modal Stall Phenomenon in a Low-Speed Axial Compressor,' ASME Journal of Turbomachinery Vol. 120,No. 3. pp. 393-401